Self-diffraction of continuous laser radiation in a disperse medium with absorbing particles

Angelsky, O. V.; Bekshaev, A. Ya.; Maksimyak, P. P.; Maksimyak, A. P.; Hanson, Steen Grüner; Zenkova, C. Yu.

Published in:
Optics Express

Link to article, DOI:
10.1364/OE.21.008922

Publication date:
2013

Document Version
Publisher's PDF, also known as Version of record

Self-diffraction of continuous laser radiation in a disperse medium with absorbing particles

O. V. Angelsky,[1,*] A. Ya. Bekshaev,[2] P. P. Maksimyak,[1] A. P. Maksimyak,[1] S. G. Hanson,[3] and C. Yu. Zenkova[4]

[1]*Correlation Optics Department, Chernivtsi National University, 2, Kotsyubinsky Str., Chernivtsi 58012, Ukraine*
[2]*Physical Department, Odessa I.I. Mechnikov National University, Dvorianska 2, Odessa 65082, Ukraine*
[3]*DTU Fotonik, Department of Photonics Engineering, DK-4000 Roskilde, Denmark*
[4]*Department of Optics and Spectroscopy, Chernivtsi National University, 2, Kotsyubinsky Str., Chernivtsi 58012, Ukraine*
*angelsky@itf.cv.ua

Abstract: We study the self-action of light in a water suspension of absorbing subwavelength particles. Due to efficient accumulation of the light energy, this medium shows distinct non-linear properties even at moderate radiation power. In particular, by means of interference of two obliquely incident beams, it is possible to create controllable phase and amplitude gratings whose contrast, spatial and temporal parameters depend on the beams' coherence and power as well as the interference geometry. The grating characteristics are investigated via the beams' self-diffraction. The main mechanism of the grating formation is shown to be thermal, which leads to the phase grating; a weak amplitude grating also emerges due to the particles' displacements caused by the light-induced gradient and photophoretic forces. These forces, together with the Brownian motion of the particles, are responsible for the grating dynamics and degradation. The results and approaches can be used for investigation of the thermal relaxation and kinetic processes in liquid suspensions.

OCIS codes: (260.2160) Energy transfer; (260.5430) Polarization; (350.4855) Optical tweezers or optical manipulation; (350.4990) Particles.

References and links

1. S. A. Akhmanov, A. P. Sukhorukov, and R. V. Khokhlov, "Self-focusing and diffraction of light in a nonlinear medium," Sov. Phys. Usp. **10**(5), 609–636 (1968).
2. D. A. Hutchins, "Mechanisms of pulsed photoacoustic generation," Can. J. Phys. **64**(9), 1247–1264 (1986).
3. V. E. Gusev and A. A. Karabutov, *Laser Optoacoustics* (AIP, 1993)
4. S. M. Avenesyan, V. E. Gusev, and N. I. Zheludev, "Generation deformation waves in the process of photoexcitation and recombination of nonequilibrium carriers in silicon," Appl. Phys., A Mater. Sci. Process. **40**(3), 163–166 (1986).
5. D. N. Auston, D. J. Bradley, A. J. Campillo, K. B. Eisenthal, E. P. Ippen, D. von der Linde, C. V. Shank, and S. L. Shapiro, *Ultrashort Light Pulses: Picosecond Technique and Applications* (Springer-Verlag, 1977)
6. S. A. Akhmanov, V. A. Vysloukh, and A. S. Chirkin, "Self-action of wave packets in a nonlinear medium and femtosecond laser pulse generation," Sov. Phys. Usp. **29**(7), 642–647 (1986).
7. V. L. Vinetskii, N. V. Kukhtarev, S. G. Odulov, and M. S. Soskin, "Dynamic self-diffraction of coherent light beams," Sov. Phys. Usp. **22**(9), 742–756 (1979).
8. O. V. Angelsky, S. B. Yermolenko, C. Yu. Zenkova, and A. O. Angelskaya, "Polarization manifestations of correlation (intrinsic coherence) of optical fields," Appl. Opt. **47**(29), 5492–5499 (2008).
9. O. V. Angelsky, M. P. Gorsky, P. P. Maksimyak, A. P. Maksimyak, S. G. Hanson, and C. Yu. Zenkova, "Investigation of optical currents in coherent and partially coherent vector fields," Opt. Express **19**(2), 660–672 (2011).
10. E. V. Ivakin, I. P. Petrovich, and A. S. Rubanov, "Self-diffraction of radiation by light-induced phase gratings," Sov. J. Quantum Electron. **3**(52), (1973).
11. A. Ashkin, "Acceleration and trapping of particles by radiation pressure," Phys. Rev. Lett. **24**(4), 156–159 (1970).
12. A. Ashkin, J. M. Dziedzic, J. E. Bjorkholm, and S. Chu, "Observation of a single-beam gradient force optical trap for dielectric particles," Opt. Lett. **11**(5), 288–290 (1986).

#184869 - $15.00 USD Received 4 Feb 2013; revised 20 Mar 2013; accepted 23 Mar 2013; published 4 Apr 2013

13. A. Ya. Bekshaev and A. I. Karamoch, "Spatial characteristics of vortex light beams produced by diffraction gratings with embedded phase singularity," Opt. Commun. **281**(6), 1366–1374 (2008).
14. M. Abramovitz and I. Stegun, eds., *Handbook of Mathematical Functions,* Applied Mathematics Series (National Bureau of Standards, 1964), Vol. 55.
15. S. H. Simpson and S. Hanna, "Orbital motion of optically trapped particles in Laguerre-Gaussian beams," J. Opt. Soc. Am. A **27**(9), 2061–2071 (2010).
16. A. N. Rubinov, "Physical grounds for biological effect of laser radiation," J. Phys. D Appl. Phys. **36**(19), 2317–2330 (2003).
17. M. Nieto-Vesperinas, J. J. Sáenz, R. Gómez-Medina, and L. Chantada, "Optical forces on small magnetodielectric particles," Opt. Express **18**(11), 11428–11443 (2010).
18. A. Y. Bekshaev, "Subwavelength particles in an inhomogeneous light field: Optical forces associated with the spin and orbital energy flows" // arXiv:1210.5730 [physics.optics] 21 Oct 2012.
19. A. Y. Bekshaev, K. Bliokh, and M. Soskin, "Internal flows and energy circulation in light beams," J. Opt. **13**(5), 053001 (2011).
20. A. Y. Bekshaev, O. V. Angelsky, S. G. Hanson, and C. Y. Zenkova, "Scattering of inhomogeneous circularly polarized optical field and mechanical manifestation of the internal energy flows," Phys. Rev. A **86**(2), 023847 (2012).
21. L. S. Ivlev and Yu. A. Dovgaliuk, *Physics of Atmospheric Aerosol Systems* (Saint-Petersburg State University, 1999)
22. V. G. Shvedov, A. S. Desyatnikov, A. V. Rode, W. Krolikowski, and Y. S. Kivshar, "Optical guiding of absorbing nanoclusters in air," Opt. Express **17**(7), 5743–5757 (2009).
23. A. S. Desyatnikov, V. G. Shvedov, A. V. Rode, W. Krolikowski, and Y. S. Kivshar, "Photophoretic manipulation of absorbing aerosol particles with vortex beams: theory versus experiment," Opt. Express **17**(10), 8201–8211 (2009).
24. N. V. Malai, "Effect of motion of the medium on the photophoresis of hot hydrosol particles," Fluid Dyn. **41**(6), 984–991 (2006).
25. C. Y. Soong, W. K. Li, C. H. Liu, and P. Y. Tzeng, "Theoretical analysis for photophoresis of a microscale hydrophobic particle in liquids," Opt. Express **18**(3), 2168–2182 (2010).
26. P. Gerstner, J. Paltakari, and P. A. C. Gane, "Measurement and modelling of heat transfer in paper coating structures," *http://www.tappi.org/Downloads/Conference-Papers/2008/08ADV/08adv26.aspx*
27. R. F. Probstein, *Physicochemical Hydrodynamics: An Introduction* (Wiley-Interscience, 2003, 2 ed.)
28. Y. Wada, S. Totoki, M. Watanabe, N. Moriya, Y. Tsunazawa, and H. Shimaoka, "Nanoparticle size analysis with relaxation of induced grating by dielectrophoresis," Opt. Express **14**(12), 5755–5764 (2006).

1. Introduction

Interaction of laser radiation with a medium containing subwavelength absorptive particles is accompanied by a set of non-linear phenomena characterized by the square-law dependence on the electromagnetic field amplitudes. They originate from diverse physical mechanisms: electro- and magnetostriction, thermal effects due to light absorption, concentration-deformation mechanism, temperature gradients, etc [1]. All the mentioned phenomena manifest themselves by induced spatial inhomogeneity of the complex refraction index and by the emergence of acoustic waves.

The striction mechanism is associated with the variations in medium density caused by modulated light flow and predominantly occurs in weakly absorbing media at high modulation frequencies [2]. If the light absorption coefficient $\alpha > 1$ cm^{-1}, and the modulation frequency does not exceed 100 MHz, the striction mechanism can be neglected in comparison to the thermal one [3]. The concentration-deformation mechanism connected with the medium density variations owing to the concentration of photoexcited charge carriers [4] plays a noticeable role only when the carriers' life time is higher than the characteristic time scale of the light intensity modulations. This preferably takes place in semiconductors exposed to picosecond laser pulses.

In the current literature, a lot of attention is paid to propagation of short high-power laser pulses in absorptive media [5–7]. Such situations seem to be the most appropriate for the research of non-linear phenomena associated with light absorption, but their applicability is limited: Because of high absorbed energy, a medium can change its physical state, up to complete destruction, which is undesirable, especially, in the study of unstable, say, organic or biological objects. Alternative approaches aimed to non-destructive experiments should be based on using continuous-wave moderate-power laser radiation. In such situations, the

#184869 - $15.00 USD Received 4 Feb 2013; revised 20 Mar 2013; accepted 23 Mar 2013; published 4 Apr 2013

technique based on formation of strongly inhomogeneous field distributions, e.g., of dynamic gratings, by means of coherent wave superposition can be advantageous [8,9].

A suitable way for studying various non-linear phenomena employs the development of amplitude and phase gratings due to heating and bleaching of absorbing solutions [10]. Additionally, in dispersed systems, the amplitude gratings can appear due to regular displacements of the suspended particles. Typical optical-field ponderomotive factors (gradient force and scattering force) act differently on dielectric and absorbing particles [11,12], respect to the field intensity gradient and the field transverse momentum (energy flow) directions. In a lot of real situations with a medium containing absorptive particles, the particles are pushed off the high-intensity field regions.

An important question is the stability of the field-induced gratings. In usual cases when short and powerful laser pulses are used, the temperature gradient and the particles' Brownian motion have no time to destroy the grating. In typical experiments exploiting continuous-wave lasers, the energy absorbed within a high-intensity region may efficiently flow away to adjacent regions via the particles' motion and due to the heat conductivity, making the induced grating disappear. However, one can expect that for certain conditions a sort of equilibrium is established and the energy outflow from the high-intensity regions is compensated by continuous supply of absorbed energy.

Of course, this requires rather efficient light absorption and dispersed systems with absorptive particles. For example, usually thermal modulation of the refraction index in water is only available at very high power of the laser radiation because of minor absorption in the visible range. In the presence of small absorptive particles, the thermal grating is formed with essentially lower laser power. The aim of the present work is to analyze, both theoretically and with experiment, the main regularities of thermal grating formation in water-based disperse systems and possible manifestations of the gratings via the incident beam self-diffraction.

2. Grating formation and self-diffraction

In this paper, our main object is the water-filled cell with suspended absorptive particles whose sizes are small enough with respect to the light wavelength. Initially, the particles are chaotically distributed and the whole cell with the particles can be treated as an optically homogeneous absorptive medium with the effective refraction index n_0 and energy absorption coefficient α. Let us consider a superposition of two coherent plane waves propagating within a thin layer of such a medium, Fig. 1. The total field amplitude distribution in the medium is described by the relation

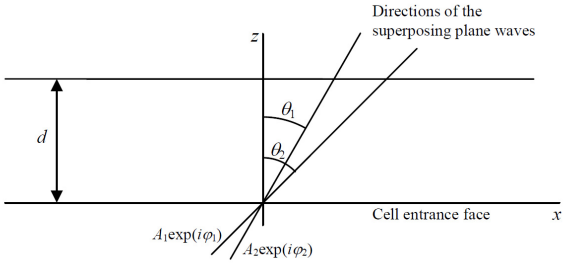

Fig.1. General model for the superposition field configuration formed in the cell.

$$A = A_1 \exp(i\varphi_1)\exp(i\Phi_1)\exp\left(-\frac{\alpha z}{2\cos\theta_1}\right) + A_2 \exp(i\varphi_2)\exp(i\Phi_2)\exp\left(-\frac{\alpha z}{2\cos\theta_2}\right), \quad (1)$$

#184869 - $15.00 USD Received 4 Feb 2013; revised 20 Mar 2013; accepted 23 Mar 2013; published 4 Apr 2013

where A_1 and A_2 are (real) amplitudes of the electric vectors of each wave and φ_1, φ_2 initial phases of the waves whose propagation axes make angles θ_1 and θ_2 with the normal to the layer surface,

$$\Phi_1 = k_0\left(x\sin\theta_1 + z\cos\theta_1\right),\ \Phi_2 = k_0\left(x\sin\theta_2 + z\cos\theta_2\right), \tag{2}$$

$k_0 = n_0 k$ is the medium wavenumber for the radiation with frequency ω, c is the velocity of light, $k = \omega/c$ is the vacuum wavenumber. In the following consideration we restrict ourselves to the symmetric case

$$\theta_1 = -\theta_2 = \theta; \tag{3}$$

then the energy density distribution of the field with amplitude (1) can be represented in the form

$$I\left(x,z\right) = g\,n_0^2\left|A\left(x,z\right)\right|^2 = I_0\left(1 + V\cos\Phi\right)\exp\left(-\frac{\alpha z}{\cos\theta}\right), \tag{4}$$

where $\varphi = \varphi_1 - \varphi_2$, g is the numerical coefficient equal to $g = \left(8\pi\right)^{-1}$ in the Gaussian system of units,

$$\Phi = \Phi_1 + \varphi_1 - \Phi_2 - \varphi_2 = 2kx\sin\theta + \varphi, \tag{5}$$

and

$$I_0 = gn_0^2\left(A_1^2 + A_2^2\right),\ V = \frac{2A_1A_2}{A_1^2 + A_2^2}. \tag{6}$$

According to Eq. (4), the light energy is inhomogeneously distributed over the medium volume and the interference grating is formed with period

$$\Lambda = \frac{\pi}{k\sin\theta}. \tag{7}$$

Now we proceed with the grating formation. Its source is the inhomogeneous distribution of the absorbed light energy; the density of the energy absorbed during the time t equals to

$$q\left(x,z,t\right) = \frac{q_0\left(t\right)}{\cos\theta}\left(1 + V\cos\Phi\right)\exp\left(-\frac{\alpha z}{\cos\theta}\right),\ q_0\left(t\right) = \alpha\frac{c}{n_0}I_0 t. \tag{8}$$

This absorption entails inhomogeneous heating of the medium which, in turn, induces a change of the refraction index, which instead of basic (zero-intensity) value $n = n_0$ is modified to $n = n_0 + \Delta n$. For the thermal mechanism of the refraction index modulation, we can express this in the form

$$\Delta n = \Delta n\left(x,z,t\right) = \left(\frac{dn}{dT}\right)\frac{q\left(x,z,t\right)}{C\rho}. \tag{9}$$

In this equation, $\left(dn/dT\right)$ is the refractive index temperature coefficient, C is the specific heat capacity (per unit mass of the medium) and ρ is the medium mass density; for simplicity, here we neglect the absorbed energy redistribution due to the heat conductivity. Subsequently,

#184869 - $15.00 USD Received 4 Feb 2013; revised 20 Mar 2013; accepted 23 Mar 2013; published 4 Apr 2013

Eqs. (8) and (9) together with (4) and (6) determine the spatial distribution of the induced medium inhomogeneity.

According to Eq. (9), the spatial profile of the refraction index explicitly depends on time. Of course, this is only correct for the initial stages of the field-medium interaction; with growing temperature gradient, the process of absorbed energy accumulation slows down due to the energy leakage to low intensity regions, and finally a stationary state with equilibrium between the absorbed and outflowing power is established. Analysis of this process is a complicated problem requiring the heat conductivity, diffusion and convection arguments and will not be conducted here. Now we note that in this stationary state, each small volume of the medium contains certain extra energy (with respect to the initial state without laser radiation) that can be called "stationary absorbed energy" (SAE). In the first approximation, it is distributed similarly to the quantity $q(x,z,t)$ so we can preserve the notation and use the function $q(x,z)$ and parameter q_0 to characterize the SAE in the same manner as Eq. (8) characterizes the transient regime of the energy absorption.

A thin layer of the medium with inhomogeneous refraction index can be considered as a phase transparency; if the layer width equals to *d*, its coordinate-dependent transmission, within a constant phase factor, is

$$T(x) = H\exp\left(ik\int_0^d \Delta n\, dz\right)\exp\left(-\frac{\alpha d}{\cos\theta}\right) \approx$$
$$H\exp\left(-\frac{\alpha d}{2\cos\theta}\right)\exp\left[i\frac{kd}{\cos\theta}\left(\frac{dn}{dT}\right)\frac{q_0}{C\rho}V\cos\Phi\right], \tag{10}$$

where *H* is an inessential constant phase factor, $|H|=1$, that will be omitted in the following analysis. The field-induced inhomogeneity of transmission (10) is a source of the self-diffraction. The spatially periodic transmission distribution can be represented via the Fourier series [13]

$$T(x) = \sum_{m=-\infty}^{\infty} T_m \exp(im\Phi), \tag{11}$$

where each term represents a certain diffraction order and coefficients T_m describe the diffracted beams' amplitudes. Because of the known relation [14] $\exp(iB\cos\Phi) = \sum_{m=-\infty}^{m=\infty} i^m J_m(B)\exp(im\Phi)$, where $J_m(B)$ is the Bessel function of the first kind, and in view of Eq. (10), the coefficients of the series (11) are determined by the equation

$$T_m = i^m J_m\left[\frac{kd}{\cos\theta}\left(\frac{dn}{dT}\right)\frac{q_0}{C\rho}V\right]\exp\left(-\frac{\alpha d}{2\cos\theta}\right). \tag{12}$$

The relative efficiency for the *m*-th order diffraction is characterized by the quantity $D_m = |T_m|^2$. Under assumption $\Delta n/n_0 << 1$, for the most interesting zero-order and first-order diffracted beams we obtain

$$D_0 = \left\{1-\frac{1}{2}\left[\frac{kd}{\cos\theta}\left(\frac{dn}{dT}\right)\frac{q_0}{C\rho}V\right]^2\right\}\exp\left(-\frac{\alpha d}{\cos\theta}\right), \tag{13}$$

#184869 - $15.00 USD Received 4 Feb 2013; revised 20 Mar 2013; accepted 23 Mar 2013; published 4 Apr 2013

$$D_1 = \frac{1}{4}\left[\frac{kd}{\cos\theta}\left(\frac{dn}{dT}\right)\frac{q_0}{C\rho}V\right]^2 \exp\left(-\frac{\alpha d}{\cos\theta}\right). \quad (14)$$

In particular, Eq. (14) testifies that the first-order diffracted intensity grows with increasing incidence angle θ. This happens due to increasing the light pathway in the self-induced grating. On the other hand, longer light pathway causes the reverse influence associated with growth of the diffracted light absorption (see the exponential multiplier in Eqs. (13) and (14)). However, in many practical situations the first factor prevails. For example, consider the following experimental conditions (Table 1).

Table 1. Experimental Conditions

1	Mean size of the pigment particles	0.2 μm
2	Concentration of the pigment particles	0.4 g·cm^{-3}
3	Absorption coefficient of the medium	$7\cdot10^2$ cm^{-1}
4	Cell thickness	10 μm (αd = 0.7)
5	Radiation wavelength	0.532 μm ($k = 1.18\cdot10^5$ cm^{-1})
6	Refractive index temperature coefficient	(dn/dT) = $0.8\cdot10^{-4}$ K^{-1}
7	Specific heat capacity (water)	4.2 kJ·kg^{-1}·K^{-1}
8	Mass density (water)	10^3 kg·m^{-3}

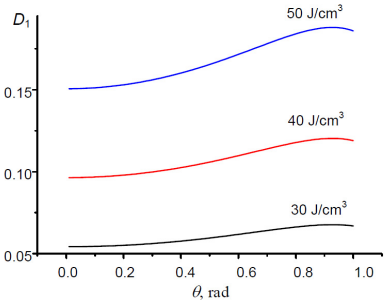

Fig. 2. First-order diffraction efficiency vs. the incidence angle for the SAE density q_0 = 30, 40 and 50 J/cm^3.

Figure 2 illustrates the incidence-angle dependence of the diffracted beam intensity for the case of $A_1 = A_2 = A$. It represents the first-order diffracted intensity normalized by the half incident intensity $gn_0^2|A|^2$, for three values of the SAE density. One can see that the self-diffraction efficiency is approximately proportional to the square of q_0, in agreement with Eq. (14); besides, it really grows with the incidence angle and reaches maximum for $\theta \cong 0.9$ rad when further increase of the diffracted power is suppressed by the radiation absorption.

3. Experimental study of the self-diffraction

3.1. Experimental technique and equipment

In the experiments, we used a water suspension of the pigment ink 10BP designed for inkjet printers. The ink particles are polymer spheres 0.2 μm in diameter with a coating made of carbon-based absorptive resin. The self-diffraction efficiency was quantitatively estimated via the quantity D_1 as a ratio of the first-order diffracted power to the power of one of the identical incident beams.

Measurements were performed with the experimental setup illustrated in Fig. 3. The semiconductor laser CASIX LDS-1500 generates radiation with wavelength λ = 532 nm, power controlled to 100 mW, and linearly polarized within the plane orthogonal to the figure

#184869 - $15.00 USD Received 4 Feb 2013; revised 20 Mar 2013; accepted 23 Mar 2013; published 4 Apr 2013

plane. The radiation traverses the telescopic system TS (two objectives with common focal plane where a micrometer-size pin-hole is placed) that produces a parallel beam with diameter 0.7 mm. A beam-splitter BS divides the laser beam in two, and the 90° angular reflectors AR1 and AR2 redirect the beams strictly backward but with a certain transverse shifts. Angular reflectors facilitate transverse displacements of the beams at the beam-splitter output without changing their path difference and make the beams interfere.

In the micro-objective focus, the intensity distribution is formed with parallel planes corresponding to the interference maxima. The diameter of the focused beams was approximately $40\,\mu m$. In the interference region, a cell of fused silica-C with the investigated medium is placed. The thickness of the cell walls is 1 mm and the working volume thickness is $10\ \mu m$. After passing through the cell, the radiation hits the screen S, if the intensity is high, or directly onto the CCD camera at low laser intensities. The plane-parallel plate PP is employed to change the path difference between the two beams by an amount greater than the coherence length of the laser radiation. This enables switching between the coherent (well-developed interference pattern) and incoherent (no interference pattern) regimes. Figure 4 shows the fields observed in the cell plane in the two cases.

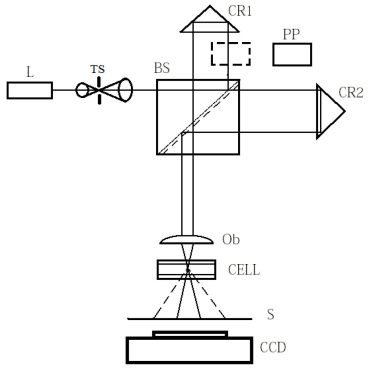

Fig. 3. Optical system for the self-diffraction investigation: (L) laser CASIX LDS-1500; (BS) beam-splitter; (CR1), (CR2) 90° angular reflectors; (Ob) micro-objective; (S) screen; (CCD) camera.

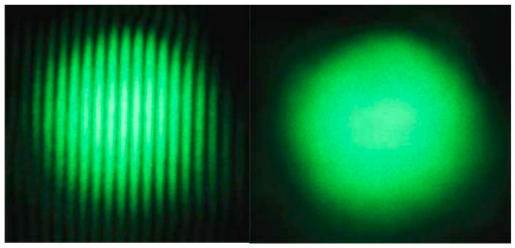

(a) (b)

Fig. 4. Resulting field formed in the cell plane when the two beams are coherent and the interference pattern is well developed (a) and when the beams are mutually incoherent (b). The interference pattern period in (a) is 2.5 μm.

In Fig. 5 examples are presented of the self-diffraction pattern observed at a distance 50 mm behind the cell. The panel (a) illustrates the self-diffraction suppression when the plane-parallel plate PP (Fig. 3) is introduced into the beam path; the other panels 5(b)–5(e) represent the diffracted beams' appearance and qualitatively characterize their intensities. As the thermal grating is a phase grating, the number of observable orders should be high; however,

#184869 - $15.00 USD Received 4 Feb 2013; revised 20 Mar 2013; accepted 23 Mar 2013; published 4 Apr 2013

only the first diffraction order is really observed (Figs. 5(b)–5(e)). This testifies that the grating cannot be considered thin, and the Bragg spatial-filtering mechanism effectively works in the rather thick disperse-medium layer.

The phase grating modulation contrast depends on the particles' concentration and the temperature gradient. The use of a thin grating would be the simplest solution for the self-diffraction modeling; however, in this case the number of particles interacting with the radiation is relatively small, and to obtain the necessary diffraction efficiency with a thin grating one should employ a higher temperature gradient than in a thick grating. Simultaneously, high temperature leads to the undesirable medium transformation, up to local phase transitions and cavitation effects. In view of this, the optimal grating thickness of 10 μm was chosen.

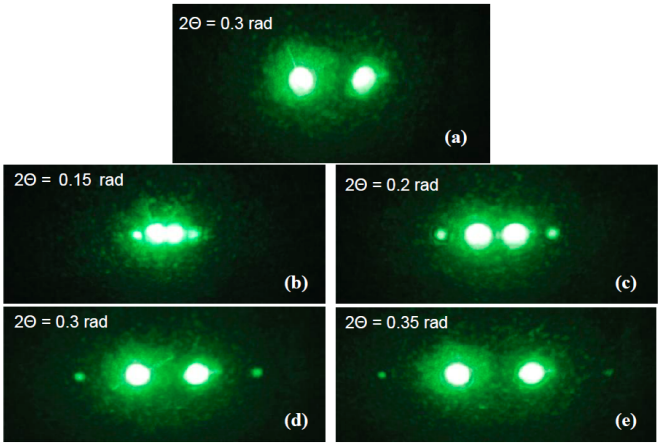

Fig. 5. Diffraction patterns observed in the screen: (a) pattern observed when the plate PP is introduced (no self-diffraction due to the lack of coherence) and (b) – (e) self-diffraction patterns at different angles of the beams' convergence as indicated.

3.2. Results and discussion

The main subject of the study was the first-order self-diffracted beam, its power and spatial characteristics. In general, there are two beams propagating in the directions of the first-order self-diffraction (dashed lines in Fig. 3). E.g., the left dashed line corresponds to the first-order diffraction of the right incident beam and to the second-order diffraction of the left incident beam. However, the second-order intensity was much lower, and could be neglected in the actual experimental conditions.

The first-order diffraction efficiency D_1 was measured as a ratio of the diffracted beam power to the power of a single incident beam. Figure 6 illustrates the observed dependence of D_1 on the incident beams' convergence angle 2θ. In contrast to the simulation results (Fig. 2), increase of the angle θ leads to decrease of the self-diffraction efficiency. This result can be caused by two effects: (i) dynamical characteristics of the induced grating formation and peculiarity of the dynamic equilibrium between the energy accumulation and dissipation in the inhomogeneously illuminated medium and (ii) partial spatial filtering of the self-diffraction orders by the thick grating. The first reason is associated with the Brownian motion of the suspended particles and will be discussed in Sec. 4.2 below; the role of the second one is determined by the parameter of the grating thickness

$$Q = \frac{2\pi d\lambda}{n\Lambda^2}. \tag{15}$$

#184869 - $15.00 USD Received 4 Feb 2013; revised 20 Mar 2013; accepted 23 Mar 2013; published 4 Apr 2013

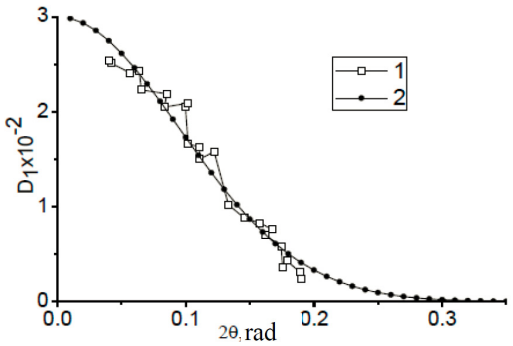

Fig. 6. First-order self-diffraction efficiency vs. the angle of the incident beams' convergence: experimental points (squares) are confronted with the approximation solid curve obtained via Eqs. (28), (35) with t_0 = 80 ms.

In our experiments, the interference pattern period Λ varied from 2.5 to 10 μm so that for $d = 10$ μm the parameter Q was within the limits 0.25 to 4. This testifies that the condition of thick Bragg grating $Q > 5$ is not fulfilled and the grating cannot be considered thick. However, certain influence of the grating thickness was yet perceptible. One can notice an inessential decrease of the first-order intensity due to the partial space-time frequency filtering and the total filtering of the higher diffraction orders with growing diffraction angles when the grating thickness approaches the "thick grating" conditions.

4. Motion of the particles and the grating dynamics

The experimental results demonstrate that as long as the incident radiation is continuous, the observed diffraction pattern is temporally stable and the self-diffraction process possesses a stationary character. However, this stable behavior is a result of dynamical equilibrium: the temperature distribution is maintained inhomogeneous and intensities of the diffraction orders do not vary while the energy of the incident radiation is permanently absorbed and dissipated.

The light-induced temperature inhomogeneity is immediately responsible for the phase grating studied in the previous sections. That is why, in the performed analysis, the distribution of the pigment particles over the cell volume was assumed homogeneous and independent on the light field. However, this is a rather coarse approximation. In fact, the field and temperature inhomogeneity provokes the spatial redistribution of the particles [9,15]; regarding the field characteristics and the particles' nature, they can accumulate near the minima or maxima of the interference pattern thus forming an amplitude grating accompanying the 'primary' phase grating. Additionally, the particles perform stochastic Brownian motion that could induce fluctuations in the diffraction conditions and, hence, in spatial profiles of the diffracted beams.

Besides, possible motion of the particles, both field-induced and stochastic, plays an important role in the thermal grating formation, maintenance and degradation. This is supported by our experimental observations: When the interference pattern period is comparable with the mean free-path length of the Brownian particles or with the effective thermal diffusion length, the grating is destroyed and the self-diffraction efficiency vanishes.

The process of spatial redistribution of the suspended particles due to the mechanical action of the interference optical field was studied in many details by Rubinov [16]. However, he dealt with rather coarse non-absorbing particles whose sizes were comparable with the grating period. In such conditions, the thermal effects in the cell volume as well as the role of the particle's Brownian motion were negligible. The full theoretical analysis of the grating dynamics and degradation processes is rather sophisticated. In this Section, we consider the

#184869 - $15.00 USD Received 4 Feb 2013; revised 20 Mar 2013; accepted 23 Mar 2013; published 4 Apr 2013

main factors involved in our conditions and qualitatively discuss their relative weights and meaning.

4.1. Field-induced mechanical action

Along with absorption of the light energy, the particles experience a ponderomotive action due to the inhomogeneous optical field. We may estimate this action analytically in the dipole approximation which is acceptable if the particle radius a satisfies $ka << 1$. In this case the electromagnetic field exerts on a non-magnetic particle with electric polarizability α_e the dipole force [15–18]

$$\mathbf{F}_e = \frac{1}{4gn_0^2}\mathrm{Re}(\alpha_e)\nabla I + \frac{\omega}{g}\mathrm{Im}(\alpha_e)\mathbf{p}_O^e, \tag{16}$$

where $I \equiv I(x,z)$ is the field energy density - in our case described by relation (4) - and

$$\mathbf{p}_O^e = \frac{g}{2\omega}\mathrm{Im}\left[\frac{1}{\mu}\mathbf{E}^* \cdot (\nabla)\mathbf{E}\right] \tag{17}$$

is the electric part of the field orbital momentum [18,19], **E** being the electric vector of the field. The polarizability α_e is characterized by the relations [18,19]

$$\alpha_e = \frac{\alpha_e^0}{1 - i\frac{2}{3\varepsilon}k^3\alpha_e^0} \approx \alpha_e^0 + i\frac{2}{3\varepsilon}k^3\left|\alpha_e^0\right|^2, \tag{18}$$

$$\alpha_e^0 = \varepsilon a^3 \frac{\varepsilon_p - \varepsilon}{\varepsilon_p + 2\varepsilon}, \tag{19}$$

where $\varepsilon = n_0^2$ and ε_p are the medium and particle permittivity, respectively. In the field formed by interference of two plane waves with $A_1 = A_2$, with symmetrical incidence (Eq. (3) holds), the orbital momentum $\mathbf{p}_O^e$ is directed exactly along the z-axis [20] and the second term of (16) makes no contribution to the transverse motion of the particles. A possible z-directed motion is prevented by the cell structure and plays no important role in the experimental behavior.

Therefore, the only transverse action is that associated with the gradient force expressed by the first term of Eq. (16). Without loss of generality we may consider a particle situated near the cell surface ($z = 0$), where the force can be evaluated via the equation

$$F_e(x) = -I_0\frac{ka^3}{2g}\mathrm{Re}\left(\frac{\varepsilon_p - \varepsilon}{\varepsilon_p + 2\varepsilon}\right)\sin(2kx\sin\theta + \varphi)\sin\theta, \tag{20}$$

which follows directly from Eqs. (16), (17), (18) and (4), (5) and coincides with the gradient force used in [16]. A numerical estimation requires knowledge of the particle dielectric properties. The pigment particles used in our experiments are nearly spherical with mean radius $a = 0.1\,\mu\mathrm{m}$ and contain ~20 nm absorptive coating of carbon-based resin. Assuming the complex refraction index of the coating to be close to that of the atmospheric soot, we accept the following values of the particle and medium (water) parameters [21]:

$$n_p = 1.82 + 0.74\mathrm{i},\ \varepsilon_p = n_p^2 = 2.76 + 2.69\mathrm{i},\ \varepsilon = 1.33^2 \simeq 1.77. \tag{21}$$

#184869 - $15.00 USD Received 4 Feb 2013; revised 20 Mar 2013; accepted 23 Mar 2013; published 4 Apr 2013

Another reason for the particle transverse motion, not taken into account in Ref [16], is the photophoresis force owing to inhomogeneous heating a particle by the absorbed radiation. Mechanisms for the photophoretic action and means for their analysis are mainly developed for gaseous media [22,23]; the theory of photophoresis in liquids is not well elaborated and only a few attempts were made in this field [24,25]. For rough estimations, we use a simplified calculation scheme based on combination of approaches presented in Refs [23]. and [25]. We start with Eq. (17) of Ref [25]. which gives the photophoresis velocity V_p of a particle and define the corresponding photophoretic force F_p via Stokes formula

$$F_p = 6\pi a \eta V_p, \tag{22}$$

where η is the water viscosity. Then we take the asymmetry factor J_1 [23,25] in the form $J_1 = -(2/3)a\alpha_p$ [23], where

$$\alpha_p = 2k \operatorname{Im}(n_p) \tag{23}$$

is the light absorption coefficient of the particle, and assume the particle to be non-hydrophobic (the 'slip length' L_s in [25]). After some manipulations, the photophoretic force can be represented by the expression

$$F_p = -\kappa \pi a^2 P, \tag{24}$$

where

$$\kappa = \frac{2}{9}\frac{\beta_T A_H r_0^2}{v_0}\frac{\alpha_p}{\chi_p + 2\chi} \tag{25}$$

is an analog of the coefficient κ introduced by Eq. (8) of Ref [23], which characterizes the momentum transfer from the liquid molecules to the particle with given properties, $P = (c/n_0)I$ is the energy flow density in the incident light field supposed to be a plane wave in [25]. In Eq. (25) β_T is the cubic thermal expansion coefficient of the medium, A_H is the Hamaker constant, r_0 is the radius of the medium molecule, v_0 is the specific molecular volume, χ and χ_p are the thermal conductivities of the medium and the particle, respectively. Then, following [23], the result (24) is generalized to the case of the transverse force in an inhomogeneous incident field via the replacement

$$\pi a^2 P \to \int_{S_+} \frac{\mathbf{r}}{a} P(\mathbf{r})\, dS, \tag{26}$$

where the integration is performed over the projection of the particle side exposed to the incident radiation, $\mathbf{r}$ is the 2D radius-vector originating from the particle center projection, $P(\mathbf{r}) \approx (c/n_0)I(x,z)$ is the incident beam power density (the explicit z-dependence reflects change of the incident radiation with the cell depth but for rough estimates we still assume $z = 0$).

Again, we employ expressions (4) and (5) with $V = 1$ and, introducing polar coordinates in the transverse plane and taking $z = 0$, evaluate integral (26) as follows:

#184869 - $15.00 USD Received 4 Feb 2013; revised 20 Mar 2013; accepted 23 Mar 2013; published 4 Apr 2013

$$\int_{S_+}\frac{\mathbf{r}}{a}P(\mathbf{r})\,dS=\frac{c}{an_0}\int_0^a\int_0^{2\pi}r\begin{pmatrix}\cos\phi\\ \sin\phi\end{pmatrix}I(r,\phi)\,r\,dr\,d\phi=$$
$$\frac{c}{an_0}I_0\int_0^a r^2dr\int_0^{2\pi}\begin{pmatrix}\cos\phi\\ \sin\phi\end{pmatrix}\cos(2kr\sin\theta\cos\phi+\varphi)\,d\phi. \tag{27}$$

This result is in the form of a column vector whose elements represent the x- and y-components of the force. Due to the symmetry, the y-component vanishes and the whole force (24) is directed along the x-axis. As a result, Eq. (24) and elementary transformations of (27) yield the final expression for the photophoretic force

$$F_p(x)=\pi a^2I_0\frac{c}{n_0}\kappa\sin(2kx\sin\theta+\varphi)\frac{J_2(2ka\sin\theta)}{ka\sin\theta}$$
$$\approx\frac{\pi}{2}I_0\frac{c}{n_0}ka^3\kappa\sin(2kx\sin\theta+\varphi)\sin\theta, \tag{28}$$

where J_2 is the symbol of the Bessel function. The second line of the equation represents an approximation valid when the particle is small with respect to the period of the interference pattern ($ka\sin\theta<<1$).

For latex particles with carbon coating suspended in water, $\beta_T=2.57\cdot10^{-4}$ K^{-1}, $A_H=5.0\cdot10^{-20}$ J, $r_0=1.54$ Å, $\nu_0=30$ Å^3, $\chi=0.61$ W/(m K) [25] and $\chi_p=0.55$ W/(m K) [26], and after evaluating α_p from Eqs. (20) and (22) one finds $\kappa=2.1\cdot10^{-8}$ s/m. The spatial dependence of the forces F_p and F_e for $a=0.1$ μm , $\theta=3.0°$ and $\varphi=0$ (see Eqs. (20) and (28)) is illustrated by Fig. 7. It expectedly shows that both forces are comparable in magnitudes but opposite in sign: the gradient force pulls the particle towards the interference maxima while the photophoretic one promotes the particles to move to the low-intensity regions. The 'net' field-induced mechanical action is dictated by the prevailing photophoretic force (note that possible hydrophobic properties of the particles may only increase the photophoretic effect [25]).

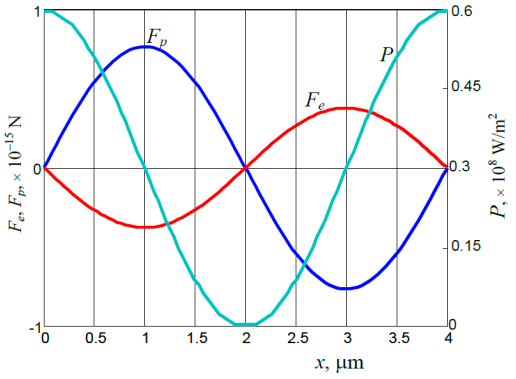

Fig. 7. Spatial dependence of the light intensity P (right scale), gradient F_e and photophoretic F_p force (left scale) within a single period of the interference pattern for $\theta=3.0°$ and $I_0=1.33\cdot10^{-1}$ J/m^3 (peak intensity $6\cdot10^7$ W/m^2). The particle parameters are described in the text (see also Eq. (20)).

#184869 - $15.00 USD Received 4 Feb 2013; revised 20 Mar 2013; accepted 23 Mar 2013; published 4 Apr 2013

4.2. Stability and degradation of the self-induced grating

The above-described mechanisms of formation and evolution of the self-induced grating show that the grating instability as well as its stationary pattern is essentially influenced by the heat conductivity and by the motion of the pigment particles from 'hot' regions to 'cold' ones. Along with the chaotic diffusion-like redistribution of particles caused by molecular mechanisms, the electromagnetic field-induced ponderomotive action provides regular drift-like displacements of the particles that contribute to the creation of the additional amplitude grating.

To evaluate the possible behavior of the particles due to the factors mentioned we performed the numerical simulation of the motion of a single suspended particle. The process is considered as a discrete Marcovian chain with updating the particle coordinates after each step of the fixed duration τ. Due to Brownian motion, at *i*-th step the particle's *x*-coordinate obtains a random increment $(\Delta x_i)_{rand}$ distributed normally with the root-mean-square value $\sqrt{2D_f\tau}$ where

$$D_f = \frac{k_B T}{6\pi\eta a_H} \tag{29}$$

is the diffusion coefficient. In Eq. (29) k_B is the Boltzmann constant, T is the absolute temperature and $a_H \simeq a$ is the hydrodynamic radius of the particle. Besides, the particle performs a regular drift owing to the ponderomotive action of the field. Assuming the drift velocity to be regulated by the Stoke's law (22), one finds the particle regular displacement during the *i*'th step caused by the local gradient and photophoretic forces (20) and (28),

$$(\Delta x_i)_{reg} = \frac{F_p(x_{i-1}) + F_e(x_{i-1})}{6\pi a\eta}\tau. \tag{30}$$

Here an assumption has been made that the single-step displacement is small enough so on the whole path the forces acting on the particle are the same and are determined by the position reached by the particle in the previous step. The resulting coordinate of the particle after M steps is calculated as a sum of displacements performed at all the consecutive steps,

$$x_N = x_0 + \sum_{i=1}^{M}\left[(\Delta x_i)_{rand} + (\Delta x_i)_{reg}\right]. \tag{31}$$

The particle motion was limited between two planes orthogonal to the *x*-axis and separated by two periods of the interference pattern, $x_i \in (-\Lambda, \Lambda)$. If at some step the calculated x_i gets outside the simulation region, the periodic boundary conditions were employed: $x_i \to x_i \pm 2\Lambda$.

During the simulation, the step duration was assumed to be $\tau = 1\ \mu s$, and the behavior of 10^5 particles was calculated; initially ($i = 0$) the particles were uniformly distributed over the modeled volume. The results are presented in Fig. 8. It is seen that the particles are, indeed, concentrated near the interference minima thus forming the amplitude grating which may act together with the phase of thermal origin. Note that under the accepted conditions, the mean value of $(\Delta x_i)_{reg}$ is $5.5\cdot10^{-10}$ μm or $11\cdot10^{-10}$ μm for the incident beam power 40 and 80 mW (the interference pattern peak intensity $6\cdot10^7$ W/m^2 and $12\cdot10^7$ W/m^2), respectively, while $(\Delta x_i)_{rand} = 2.1\cdot10^{-3}$ μm, which satisfies the requirement for the validity of Eq. (29) for the presumed grating period $\Lambda = 4$ μm. The regular constituent of the particle motion is

#184869 - $15.00 USD Received 4 Feb 2013; revised 20 Mar 2013; accepted 23 Mar 2013; published 4 Apr 2013

obviously much smaller than the stochastic fluctuations but the tendency to form the regular periodic distribution of particles is nevertheless quite perceptible. However, the Brownian motion permanently acts against this tendency, and limits available contrast of the amplitude grating. In the equilibrium state that is established after more than $2\cdot10^5$ steps (which corresponds to 0.2 s), the particles' density varies within 5 to 10 percents, according to the incident power (see Figs. 8(c), 8(c'), 8(d) and 8(d')).

It is interesting to compare the simulated patterns of Fig. 8 with the averaged distribution of particles calculated analytically by means of the one-dimensional Nernst – Plank equation [27]

$$\frac{\partial N}{\partial t} = D_f \frac{\partial^2 N}{\partial x^2} - \frac{1}{k_B T} \frac{\partial}{\partial x}\left(NF \right). \tag{32}$$

Here N is the particles' concentration,

$$F = F_e + F_p = F_0 \sin\left(2kx \sin\theta + \varphi \right) \tag{33}$$

is the total transverse force and, according to Eqs. (20) and (28)

$$F_0 = \frac{\pi}{2} I_0 k a^3 \sin\theta \left[\frac{c}{n_0} \kappa - 8\,\mathrm{Re}\left(\frac{\varepsilon_p - \varepsilon}{\varepsilon_p + 2\varepsilon} \right) \right].$$

The stationary solution of this equation corresponding to zero time derivative in Eq. (32) can be easily found in the form [16]

$$N\left(x \right) = N_0 \exp\left[-\frac{F_0 \cos\left(2kx \sin\theta + \varphi \right)}{2 k_B T\, k \sin\theta} \right] \tag{34}$$

(the normalization factor N_0 is determined from the condition that the total number of particles $\int N\left(x \right) dx$ is always the same and equal to the initial number of particles). The average distribution of Eq. (34) is illustrated by yellow lines in Figs. 8(d) and 8(d'). The obvious difference between the simulated and analytical results testifies for another important property of the field-induced particle distribution: generally, it is not stationary and experiences strong random deformations due to stochastic fluctuations. This fact, which invoked no important consequences in conditions of Ref [16] because large particles were rather regularly arranged within the interference fringes, is generally responsible for the non-stationary and fluctuating character of the field-induced amplitude grating. Absence of perceptible fluctuations in the experimental self-diffraction patterns serves as an additional indirect confirmation of the relative weakness of the amplitude-grating effects.

In general, Fig. 8 along with the discussion of Sec. 4.1 confirms our conclusion that in real experimental conditions the role of the amplitude grating was not essential. Its single reliable manifestation was a slightly suppressed absorption of the incident light in case of well-developed interference pattern, compared to the case of incoherent superposition of the two beams (see Sec. 3.1). In full agreement with the simulation results, experimentally we could not detect a noticeable contribution of the amplitude grating to the diffraction efficiency up to beam powers of 50 – 100 mW. On the other hand, the data of Fig. 8 and Eq. (34) suggest that the amplitude grating could be more perceptible at higher intensities but in reality the beam power of 100 mW or more appeared to be inappropriate because under such circumstances the processes of the pigment melting, local boiling of water and cavitation effects become essential. In the whole range of conditions available in our experiments, the amplitude grating was rather weak. This conclusion is additionally supported by the self-diffraction pattern (Fig.

#184869 - $15.00 USD Received 4 Feb 2013; revised 20 Mar 2013; accepted 23 Mar 2013; published 4 Apr 2013

5) where higher-order diffracted beams are absent and by the negligible level of additional fluctuations in the diffracted beam profiles caused by the Brownian motion of the particles. In all cases, the first-order intensity distribution appears to be similar to the zero-order intensity, which confirms the predominantly phase character of the grating.

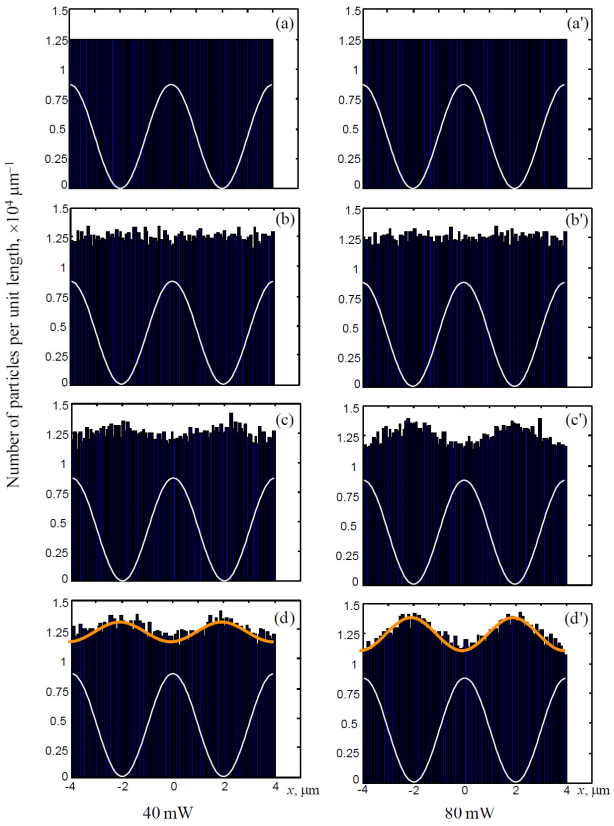

Fig. 8. Histograms of the particles' distribution along x-axis (integrated over the y- and z-directions) within a two-period fragment of the interference pattern (white line shows the light energy distribution) for the single-beam power 40 mW (left column) and 80 mW (right column): (a), (a') initial distribution of the total of 10^5 particles (homogeneous); (b), (b') after $2 \cdot 10^4$ steps (the amplitude grating is not yet developed); (c), (c') after $16 \cdot 10^4$ steps; (d), (d') after $30 \cdot 10^4$ steps (pattern corresponding to dynamical equilibrium). Total number of particles is 10^5, the step duration accepted $\tau = 1$ μs, other conditions are the same as specified in Sec. 4.1 and Fig. 7. Yellow lines in panels (d) and (d') describe corresponding averaged distributions analytically calculated via Eq. (34).

All the mentioned facts clearly indicate that the field-induced ponderomotive action cannot cause a noticeable distortion or destruction of the self-induced thermal grating described and analyzed in Sec. 2. Essential questions of the thermal grating development, consistency and degradation should be considered based on kinetic processes including the heat exchange, convection and thermal conductivity [27] that can be properly studied via observing the transient phenomena accompanying the grating emergence and vanishing after the laser radiation is turned off. However, important kinetic characteristics of these processes can be extracted from analysis of the stationary gratings with special attention to their relations with the grating spatial characteristics.

The main elementary kinetic process involved in the thermal grating formation is the energy exchange between a particle and the surrounding water. Since the specific heat capacity of water is much higher than the heat capacity of the particle, the latter remains 'hot'

#184869 - $15.00 USD Received 4 Feb 2013; revised 20 Mar 2013; accepted 23 Mar 2013; published 4 Apr 2013

during certain time interval t_0 after the particle has absorbed a portion of the light energy. This time interval correlates with the time of the thermal relaxation. It is difficult to estimate this time directly but it can be determined by using the kinetic properties of the whole disperse system. In fact, the time t_0 regulates the diffracted intensity dependence on the grating spatial frequency [28]:

$$D_m = D_{m0} \exp\left(-2D_f q^2 t_0\right), \tag{35}$$

where $q = 2\pi/\Lambda$ is determined by the grating period Λ, D_{m0} is the 'initial' m-order efficiency for a high grating period $\Lambda >> 2\pi\sqrt{D_f t_0}$ and the diffusion coefficient D_f is given by Eq. (29). Relations (29) and (35) explicitly connect the diffraction efficiency with molecular and kinetic characteristics of the Brownian motion of particles, which destroys the grating. In essence, they show that the grating can exist until the diffusion time $\Lambda\left(2\pi D_f\right)^{-1}$ exceeds the thermal relaxation time, and the thermal grating disappears for small enough grating period Λ.

The experimental dependence $D_1\left(\Lambda^{-1}\right)$ complies with Eq. (35) and the best fitting procedure (solid curve in Fig. 6) yields $t_0 = 80$ ms (other parameter values are $T = 300$ K, $\eta = 1.0 \cdot 10^{-3}$ Pa·s, $a_H = 0.1$ μm). A high degree of correlation between the experimental data and approximating curve supports the validity of the model chosen.

Conclusion

We have demonstrated the possibility of producing controllable phase gratings in disperse liquid media with suspended absorptive sub-wavelength particles. The grating prototype is formed by interference between two identical laser beams obliquely incident onto the medium. The light energy absorbed by the particles is transmitted to the medium thus forming the inhomogeneous temperature distribution and associated thermal grating due to the temperature dependence of the refraction index. Importantly, the light-induced grating structures are obtained with low-power continuous-wave laser radiation. We have found that the grating life time, contrast (the refraction index modulation) and, consequently, the self-diffraction efficiency are determined by the degree of coherence of the beams involved.

Mechanism and dynamical characteristics of the thermal grating formation and degradation are analyzed, and their relations with the kinetic and thermal properties of the medium and particles are discussed. The roles of the ponderomotive field action (gradient and photophoretic forces) and of the stochastic fluctuations in the medium (Brownian motion) are studied. The developed experimental approaches and the results obtained can be used for the recording and diagnostics of rapid processes in particle-medium interactions.

Finally, we would like to outline possible directions for further development of the proposed approach. First, it can be extended to multiple-beam interference configurations. This may contribute to the sharper interference fringes with corresponding enhancement of the optical field inhomogeneity. As a result, enhancement of the non-linear behavior could be expected. However, according to Section 4.2, the sharper fringes are subject to faster degradation which may neutralize the anticipated growth of the self-induced effects. On the other hand, the use of smaller suspended particles, up to the nanometer size, may be promising in view of decreasing thermal relaxation time. This will improve the grating dynamical characteristics with probable increase of its controllability and accuracy. These features could be especially useful in the study of non-stationary gratings induced in media with absorbing particles when the interfering coherent waves have unequal frequencies. In such situations, the

#184869 - $15.00 USD Received 4 Feb 2013; revised 20 Mar 2013; accepted 23 Mar 2013; published 4 Apr 2013

controllable evolution of the interference pattern will offer a new degree of freedom for the induced grating management, with a lot of interesting and promising applications.

Acknowledgments

The authors are grateful to the anonymous referee for the useful suggestions on the meaning and possible ways for further development of the approach proposed. Steen G. Hanson acknowledges the financial support from the Danish Council for Technology and Innovation under the Innovation Consortium LICQOP, grant #2416669.

#184869 - $15.00 USD Received 4 Feb 2013; revised 20 Mar 2013; accepted 23 Mar 2013; published 4 Apr 2013